Supplementary material for: "Newton's cradle-like allosteric mechanism explains regulatory RsmE RNA binding"

Esteban Finol[1], Fred F. Damberger[1], Miroslav Krepl[2], Timo Flügel[1], Priscilla Dietrich[1], Thomas C.T. Michaels[1], Beat Vögeli[3], Jiří Šponer[2], Frédéric H-T. Allain[1,*].

[1] Institute for Biochemistry, Department of Biology, ETH Zurich, 8093, Zurich, Switzerland

[2] Institute of Biophysics of the Czech Academy of Sciences, Kralovopolska 135, 61200, Brno, Czech Republic

[3] Department of Biochemistry and Molecular Genetics, University of Colorado Anschutz Medical Campus, Aurora, CO 80045, USA.

*To whom correspondence should be addressed.
Email address: allain@bc.biol.ethz.ch

Supplementary tables:

Supplementary table 1: ITC-derived binding kinetics and thermodynamics of RsmE dimer.

Conditions		Experimentally determined values				Calculated values[+]			
RNA binder	NaCl in buffer*	K_D^1 [mean±SD, nM]	K_D^2 [mean±SD, nM]	ΔH1 [mean, kcal/mol]	ΔH2 [mean, kcal/mol]	−TΔS1 [kcal/mol]	−TΔS2 [kcal/mol]	ΔG1 [kcal/mol]	ΔG2 [kcal/mol]
SL2	10 mM	0.94±0.45	22.34±3.36	-58.33	-27.08	46.02	16.65	-12.31	-10.44
SL2	30 mM	1.45±0.83	31.05±4.54	-56.38	-26.80	44.32	16.56	-12.06	-10.24
SL2	100 mM	5.71±2.21	64.23±5.27	-45.47	-26.34	34.23	16.53	-11.25	-9.81
SL2	300 mM	15.45±2.47	118.05±6.76	-31.75	-21.04	21.10	11.59	-10.66	-9.45
4bpSL2	30 mM	21.56±4.18	97.23±5.84	-39.38	-23.34	28.93	13.77	-10.46	-9.57

[+] ΔG values were calculated from the experimentally determined values by relating the association constant ($K_A = K_D^{-1}$), the experimental temperature (298.15 K) and the equilibrium constant (R) with the changes in the Gibbs free energy ($\Delta G = -RT [\ln K_A]$). TΔS values were calculated by subtracting the ΔG values from the ΔH values ($\Delta G = \Delta H - T\Delta S$). TΔS values are shown as - TΔS.

* The ITC buffer comprised 50 mM K_2HPO_4 at pH 7.2 and variable NaCl concentrations. Further details can be found in the Methods section.

Supplementary Texts:

Supplementary Text 1: On the assignment and quantification of the semi-*holo* RsmE states. (Related to Fig.2)

To assign the chemical shifts (CS) in the *apo* and semi-*holo* ^{15}N-RsmE states, we first recorded and analysed backbone-assignment (HNCACB, HNCA, HNCO, HN(CO)CA and HN(CA)CO) and side-chain assignment (3D HcCH-TOCSY) experiments at 313K. To assign some NH-CS that showed broad linewidth, backbone assignment experiments were also recorded at 305K and 308K. This approach allowed us to completely assign the *apo* RsmE state and partially assign the main semi-*holo* states. Considering that we have previously assigned the *holo* RsmE state[1], we assigned the remaining CS by comparing ^{1}H^{15}N-HSQC and backbone assignment experiments to the corresponding spectra of the *apo* and *holo* RsmE dimers. Moreover, we recorded 3-dimensional ^{15}N- and ^{13}C-resolved ^{1}H-NOESY experiments using long mixing times (150 ms) to confirm, using through space correlations, the independent assignment of both monomers in the semi-*holo* states.

To assign the additional states in the bound site of the semi-*holo* SL2 RNA-RsmE dimer complex, we first observed that one of the additional peaks in the ^{1}H^{15}N-HSQC spectrum has a similar CS to the B-E46-NH (**Supplementary Fig.2a**), which underwent a large CS perturbation upon RNA binding. We also observed that this additional NH peak was associated with CA (**Supplementary Fig.2b**) chemical shifts that are similar to those in B-E46-NH. We then followed a sequential walk in the ^{15}N-resolved ^{1}H-NOESY (**Supplementary Fig.2c**) supplemented by the more sensitive backbone assignment experiments (HNCA and HNCO) to assign the backbone of the additional state II in the bound CTDR and α-helix. We then used the assigned HN, Cα, and Hα CS as a starting point in the ^{15}N- and ^{13}C-resolved ^{1}H-NOESY and the 3D HcCH-TOCSY spectra to assign the sidechain of the additional state II. Despite the low abundance of the additional state III, resonances were identified from the similarity with state II correlations for sidechains in the 3D HcCH-TOCSY and ^{13}C-resolved ^{1}H-NOESY spectra.

To quantify the abundance of the three states observed for the CTDR and α-helix of the semi *holo* state of RsmE dimer, we integrated the ^{1}H^{13}C-HSQC peak volumes for isolated methyl groups from these structural elements of the RsmE dimer and we also measured the peak intensity of non-isolated ^{1}H^{13}C-HSQC peak. These two approaches yielded similar results. In the main text, the results of the first approach are provided.

Supplementary Text 2: Additional MD simulations. (Related to Fig.2 and Suppl. Fig.3)

To further characterize the conformational space that the SL2-bound CTDR and α-helix of RsmE dimer explore, we performed two additional sets of three MD simulations in explicit solvent. They differed from each other only in the starting conformation (**Supplementary Fig.3b**); one set started from the same starting conformation as in the initial four simulations in Supplementary Fig.3a (the Ade26-bound CTDR conformation), and the other set started from the additional conformation that was observed in the fourth of the initial MD simulations (the Ade26-detached CTDR conformation). However, these two sets of simulations structurally differed from the initial four simulations. The CTDR in these simulations was truncated to four residues (RsmE residues 56 to 59), instead of 14 residues. Residues 56 to 59 were kept because residues 57 and 58 were experimentally shown to contact Ade26[1]. We hypothesized that, by reducing the length of the CTDR, this disordered region would be able to navigate faster through the solvent. Thus, we would sample more structural exchange events between the two CTDR states during the same μs MD timescale. In the Ade26-bound CTDR simulations, we indeed observed an increase in CTDR-detachment events as well as emergence of the CTDR conformation that was used for the second set of CTDR-truncated MD simulations. On the other hand, in the Ade26-detached CTDR simulations, we observed that MD state II was quite stable on the same μs MD timescale.

Supplementary Text 3: On the fractional sodium occupancy in MD simulations of SL2 RNA-RsmE dimer. (Related to Fig.3 and Suppl.Fig.5a)

To investigate whether sodium ion bridges could mediate the interaction between SL2 RNA stem and the β3-β4 loops of RsmE dimer, a volumetric map at 1 Ångstrom resolution was built for the fractional occupancy of Sodium ions throughout the MD simulations, using the VolMap tool in the VMD software. A volumetric map is a 3D grid that contains a value at each grid point. After aligning the backbone of the RsmE dimer in the centre of the 3D grid throughout the MD simulation, each grid point (1 Ångstrom in size) in each MD frame was set to either 0 or 1, depending on whether the grid point was "occupied" by a sodium ion or not. By averaging over all frames, the fractional sodium occupancy was calculated for each grid point. Thus, in the SL2 RNA-RsmE dimer MD simulation, the averaged fractional sodium occupancy in the explicit solvent was < 0.0005. The averaged fractional sodium occupancy shielding the RsmE-SL2 complex was < 0.005. The volumetric map in the left panel of Supplementary Fig.5a is shown at a cutoff of 0.05, i.e., each green volume corresponds to grid points with a fractional sodium occupancy larger than 0.05. This approach allowed us to identify clusters of high fractional sodium occupancy. Importantly, the grid points in the Sodium cluster in proximity to β3-β4 loops (Shown in Fig.3a in the main text) have fractional sodium occupancies ranging

from 0.08 to 0.10, corresponding to a ~200× locally elevated sodium concentration compared to the bulk.

Supplementary Text 4: Evidence for partial unfolding of the empty α-helix in the semi-*holo* SL2 RNA-RsmE dimer complex. (Related to Fig.4 and Suppl.Fig.9)

Upon binding the first SL2, three amide peaks of the RsmE dimer in the first helical turn of the empty site α-helix (E-R44, E-E45 and E-E46) moved toward the centre of the $^{1}H^{15}N$-HSQC spectrum. Considering that the α-helix is extensively involved in RNA recognition, we speculated that these changes might imply a partial unfolding of the α-helix, which can lead to an impaired RNA recognition and reduced affinity of the second binding event. Secondary Cα, Cβ and CO CS report on changes in average secondary structure[2,3]. Upon binding of one SL2 RNA, several CO shifts in the empty α-helix of RsmE dimer showed smaller secondary shifts than in the apo RsmE dimer, suggesting a shift toward a less folded form in the folded-unfolded equilibrium (Left-side panel in **Supplementary Fig.9a**). Secondary Cα-Cβ shifts supported this interpretation (Right-side panel in **Supplementary Fig.9a**).

Another NMR feature of a random coil conformation is the sharpening of $^{1}H^{13}C$ peaks. As opposed to amide peaks, carbon attached hydrogen protons do not chemically exchange with the solvent and their chemical shift and peak line-shape are mainly determined by their chemical environment and their correlation time (τ_c). In a random coil conformation, amino acids show a shorter τ_c, with slower T2 relaxation and sharper line shape. The inspection of line-shape in peaks from methyl groups (I47Hγ2, I47Hδ1, I51Hγ2 and I47Hδ1) showed sharp peaks in the empty α-helix of the RsmE dimer when it is bound to one SL2 RNA. These methyl groups also changed their chemical shifts, as compared to the *apo* RsmE dimer. Their ^{1}H chemical shifts approached their corresponding RC chemical shift values (**Supplementary Fig.9b**). Taken together, the backbone carbon secondary shift quantification and the analysis of methyl group chemical shifts confirmed that, in the semi-*holo* state, the empty α-helix undergoes a partial unfolding.

Importantly, some residues in the *apo* state, e.g. E45, E46, I47 and R50, also showed broad linewidths in the $^{1}H^{15}N$-HSQC spectrum (**Supplementary Fig.8b**). These residues map to the hinge region between the β5 strand and the α-helix and to the first helical turn of the α-helix, suggesting that the α-helix undergoes conformational exchange, with an intermediate exchange regime, between a low and a high energy state in the μs-ms timescale. We can therefore infer that the observed changes in the empty α-helix of the semi-*holo* complex represents a shift of the folded-unfolded equilibrium towards a partially unfolded state.

To assess how the helical fold can be perturbed by binding of one SL2 RNA, we recorded ^{13}C-resolved NOESY experiments on the apo ^{13}C-RsmE dimer and on the ^{13}C-RsmE dimer bound to one or two SL2 RNA and searched for contacts between the α-helix and the β-sheets of the RsmE dimer. Clear NOEs between E45 in the first helical turn and S11 in the β2-strand were observed in the ^{13}C-resolved NOESY spectra of the *apo* RsmE dimer and SL2-saturated RsmE dimer (**Supplementary Fig.10**). In the NOESY spectrum of the semi holo RsmE dimer, the same NOEs were observed on the bound α-helix. However, these NOEs were absent for the empty site, suggesting that the partial unfolding of the empty α-helix, is also associated with a loss of its contact with the β-sheet of the RsmE dimer.

Supplementary Figures:

Supplementary Fig.1: The semi-*holo* SL2-RsmE dimer complex has two additional bound RsmE states.

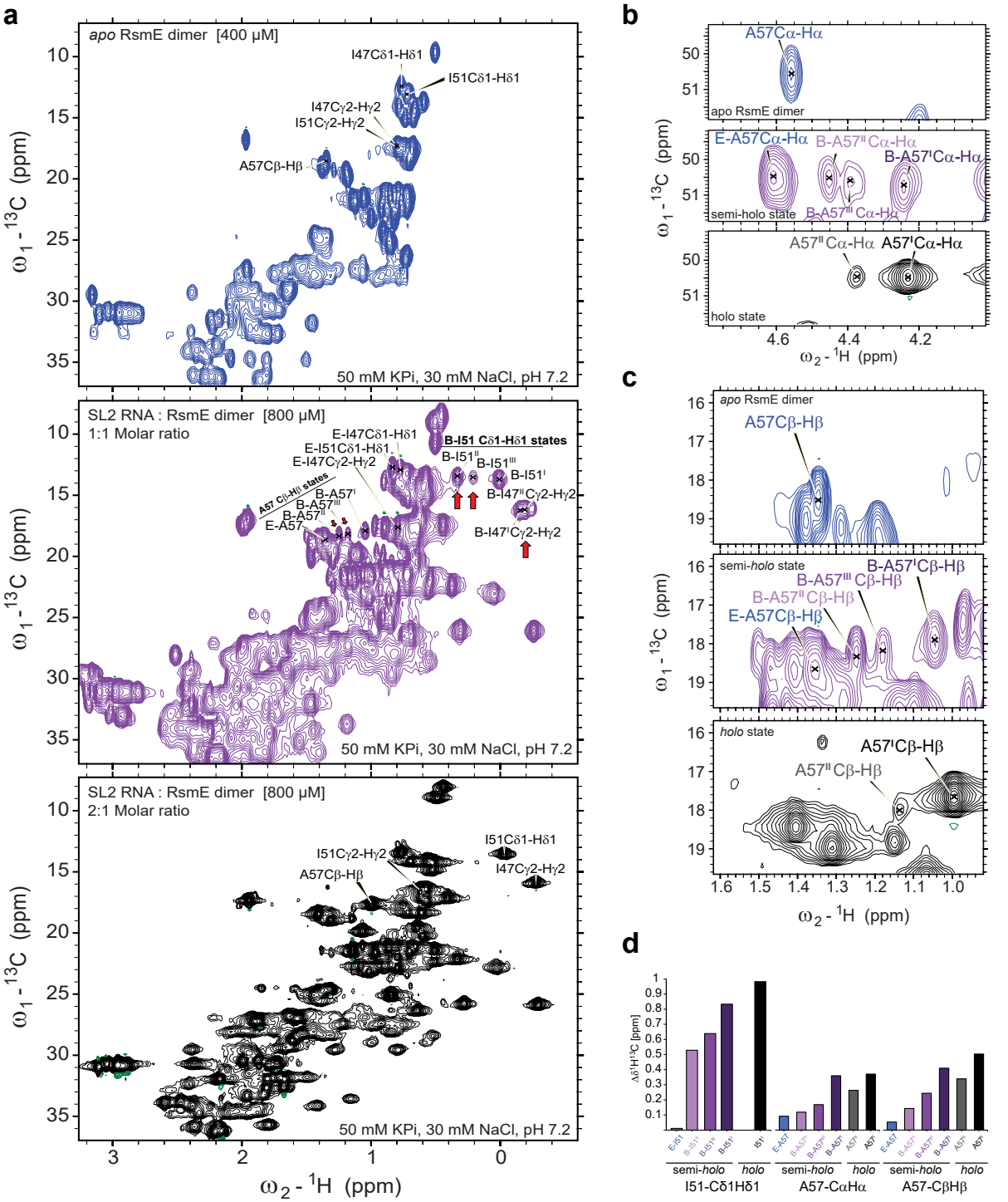

a, Methyl region of $^{1}H^{13}C$-HSQC spectra from the *apo* ^{13}C-labelled RsmE dimer (top), the semi-*holo* (middle in purple) and *holo* (bottom in black) SL2 RNA-bound RsmE dimer. Red arrows indicate the minor conformation peaks in the semi-*holo* complex. **b** & **c**, A57 CαHα and A57 Cβ-Hβ peaks of different states in $^{1}H^{13}C$-HSQC spectra. Top: the *apo* RsmE dimer. Middle: the semi-*holo* SL2-RsmE dimer complex. Bottom: the *holo* SL2-RsmE dimer complex. **d**, Bar plots with the CSP of two methyl groups in the RsmE dimer for the different conformations upon binding of one SL2 RNA: one methyl is in the α-helix (I51Cδ1-Hδ1) and the other is in the CTDR (A57Cβ-Hβ).

Supplementary Fig.2: Assignment of secondary conformations in the bound α-helix and CTDR of the RsmE dimer.

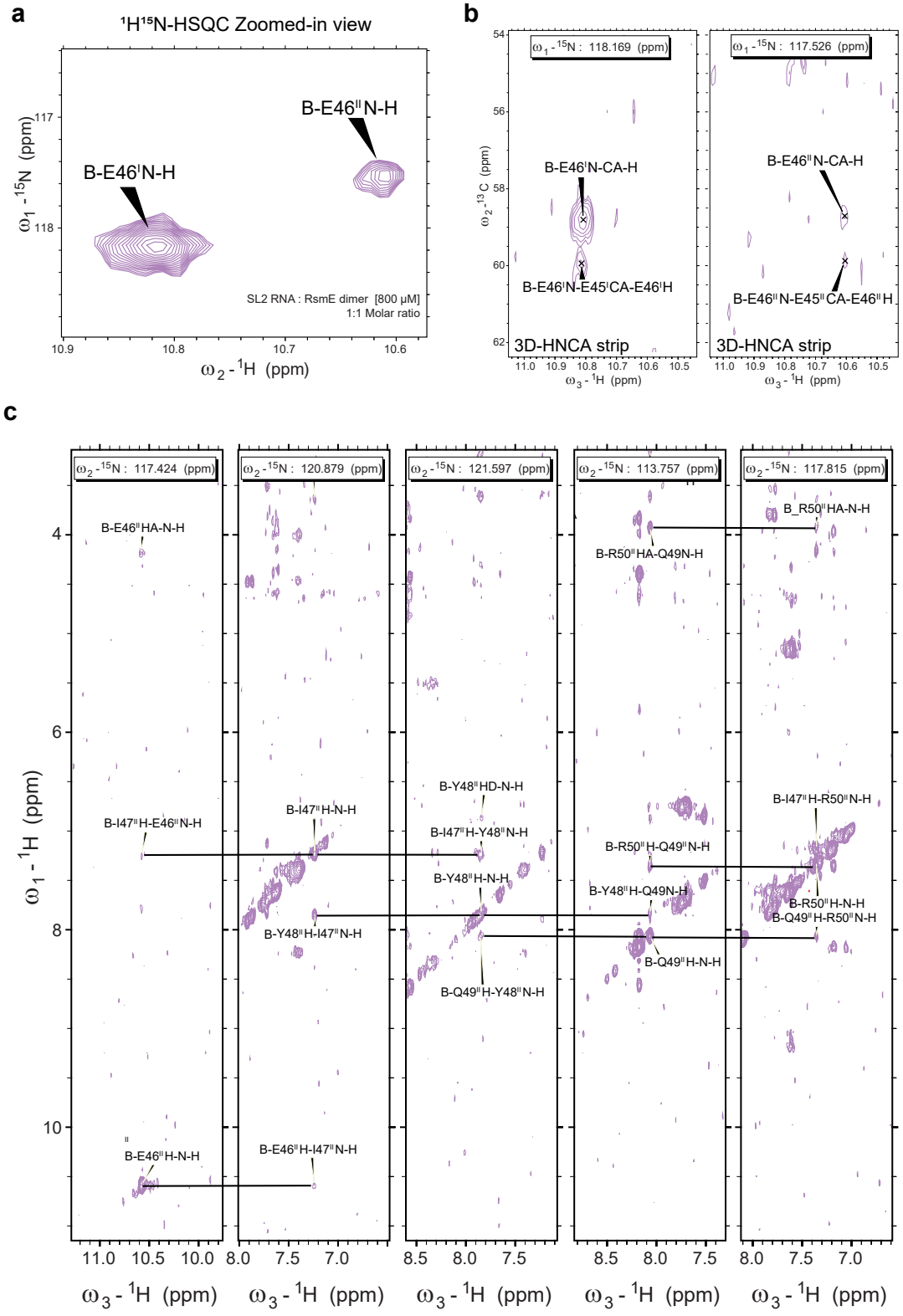

a, Region of $^{1}H^{15}N$-HSQC spectrum showing B-E46 NH peaks from the semi-*holo* SL2-RsmE dimer. **b**, Strip plots from the HNCA spectrum from the semi-*holo* RsmE dimer state. The strips are centred on the ^{15}N-CS of the major E46^{I} and minor E46^{II} backbone amide peaks. **c**, Strip plots from the three-dimensional HNH-NOESY spectrum of the RsmE dimer bound to one SL2 RNA. The five strips are centred on the NH-CS of residues 46^{II} to 50^{II} from the minor conformation of the semi-*holo* SL2-RsmE dimer complex. Black lines indicate the sequential assignment.

Supplementary Fig.3: The state II conformation is stable on the μs timescale.

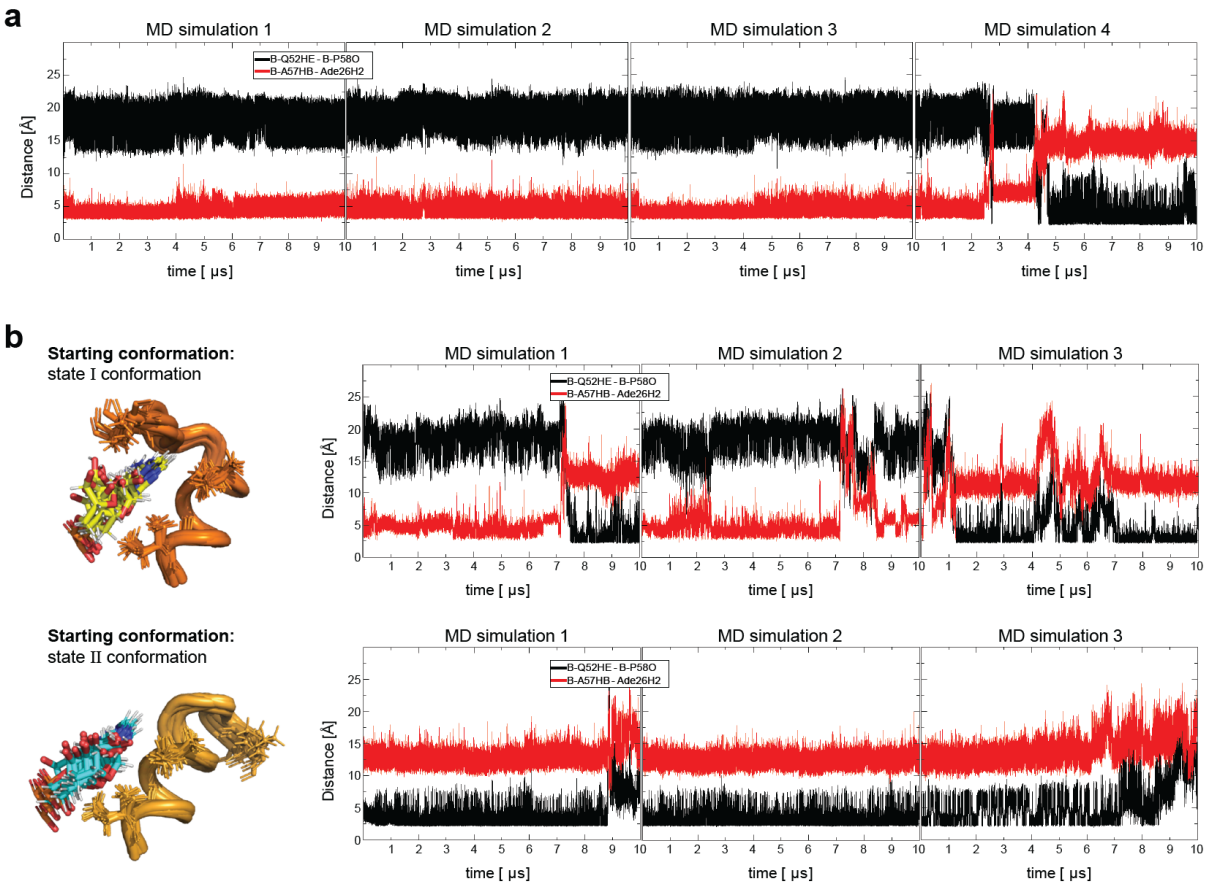

a, Evolution of the atomistic distances B-A57Qβ-Ade26H2 (red) and B-Q52Hε-P58O (black) in four MD simulations from the semi-*holo* SL2 RNA-RsmE dimer complex. **b**, Evolution of the same atomistic distances in the MD simulations that started from the Ade26-bound state I (top panel) and state II (bottom panel) conformations. The conformations of the CTDR where Adenine 26 interacts as in the SL2 RNA-RsmE dimer complex (top), and the conformation where the CTDR loses the contact to Ade26 (bottom). The measured distances are indicated by red and black lines.

Supplementary Fig.4: The minor conformation II corresponds to the MD-derived state II conformation in the CTDR of the bound RsmE dimer.

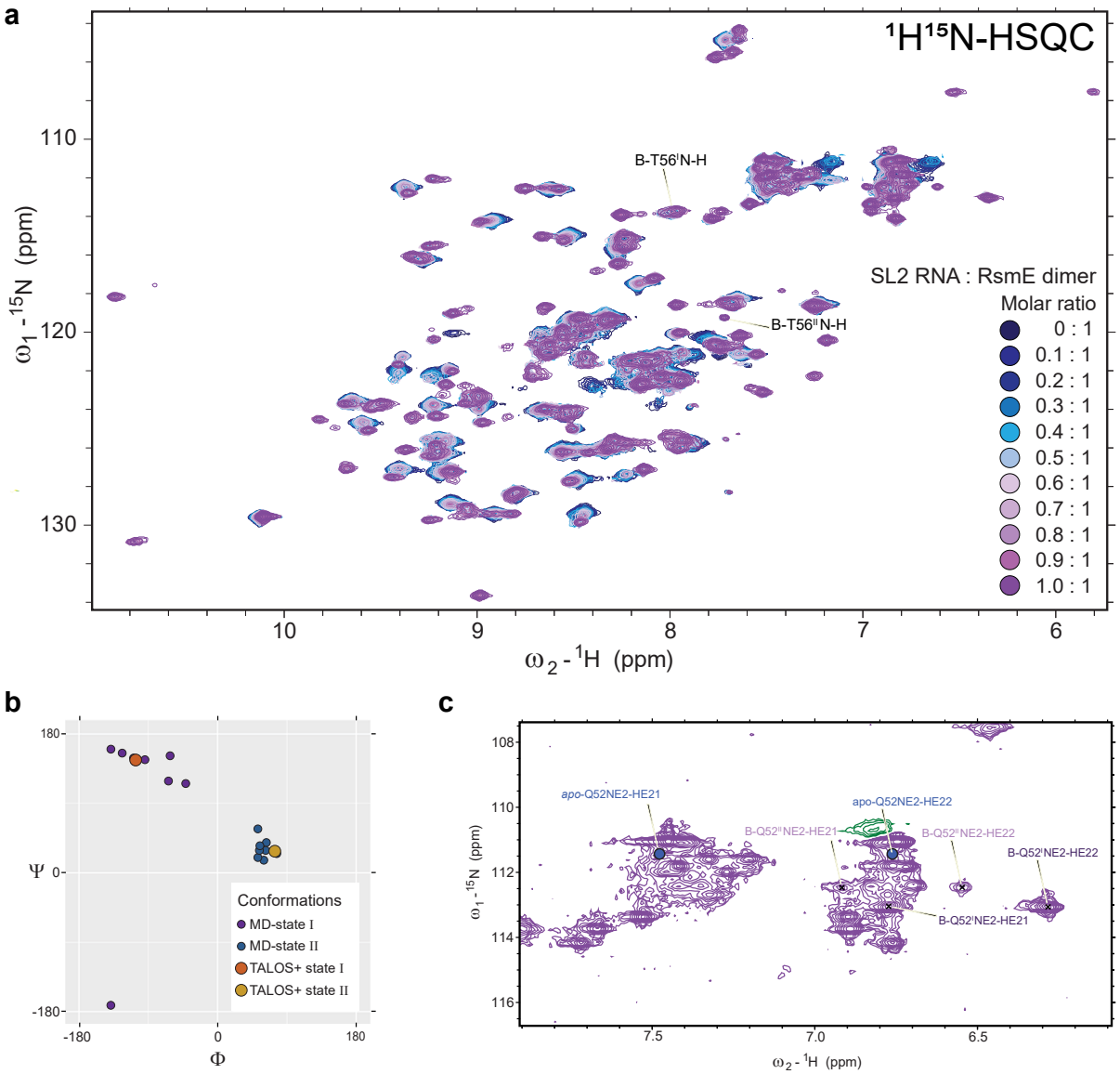

a, Overlaid ^{1}H^{15}N-HSQC spectra from the titration of SL2 RNA into the ^{15}N-RsmE dimer. In this titration, only the first binding site was saturated. As SL2 RNA concentration increased, a set of weak additional peaks emerged. Labels show the B-T56 NH-CS for the major (T56^{I}) and minor (T56^{II}) conformation. **b**, Ramachandran plot with ψ and ϕ angles for B-T56 major (state I) and minor (state II) conformations as predicted from their backbone chemical shifts (H, N, CO, CA) using TALOS+[4]. The ψ and ϕ angles were also calculated from 10 frames of MD state II missing the CTDR-Ade26 contact, and 10 frames from the canonical Ade26-bound MD state I conformation. **c**, Side chain region of the ^{1}H^{15}N-HSQC spectrum of the semi-*holo* RsmE dimer state. Distinct B-Q52 NE2-HE21 and NE2-HE22 CSs were observed for the minor conformation (state II).

Supplementary Fig.5: Transient contacts between the SL2 RNA stem and the β3-β4 loop in the empty site of the RsmE dimer were observed in MD simulations.

a

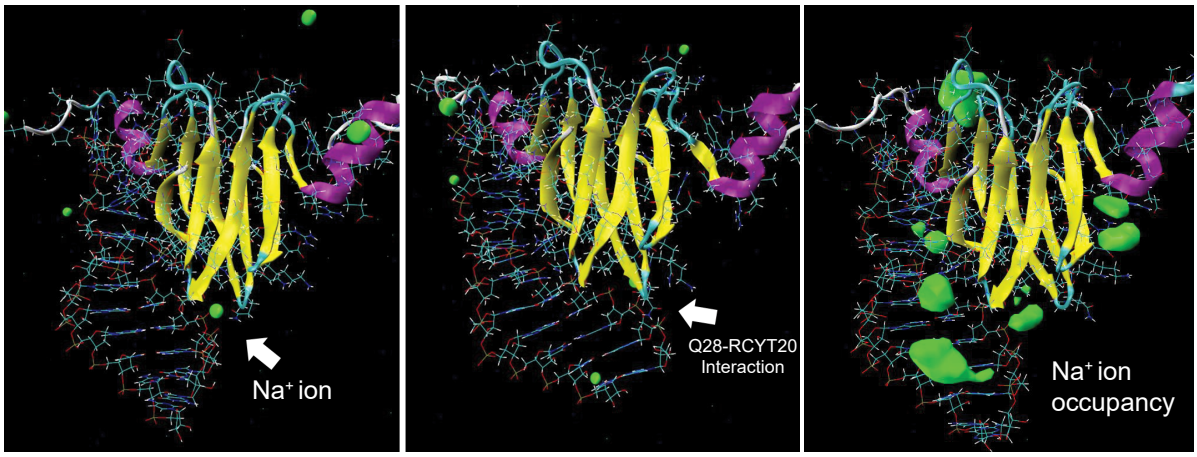

b

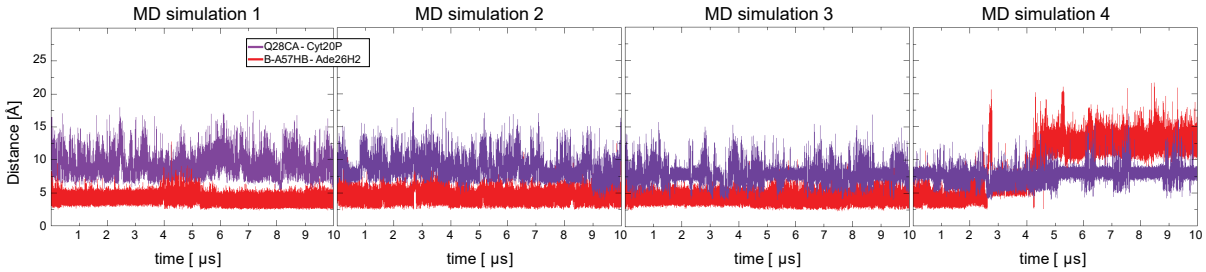

a, Snapshots from the MD simulation of the semi-*holo* SL2-RsmE dimer complex. The secondary structures of the RsmE dimer are shown with yellow (β-strand) and magenta (α-helix) ribbons. Sodium ions (Na^+) are shown as green spheres in the first two panels. The white arrows point to the "coordinated" Sodium ion in the first panel, and to the contacts between the RNA stem and the β3-β4 loop of the empty site of RsmE dimer in the second panel. The third panel shows the Sodium ion occupancy with green volumes indicating regions of higher occupancy (>5%) throughout the MD simulations. **b**, Evolution of the E-Q28Cα-Cyt20P (purple) and B-A57Qβ-Ade26H2 (red) atomistic distances in four MD simulations of the semi-*holo* SL2-RsmE dimer complex.

Supplementary Fig.6: Evidence for transient contacts between SL2 RNA stem and β3-β4 loops in RsmE dimer.

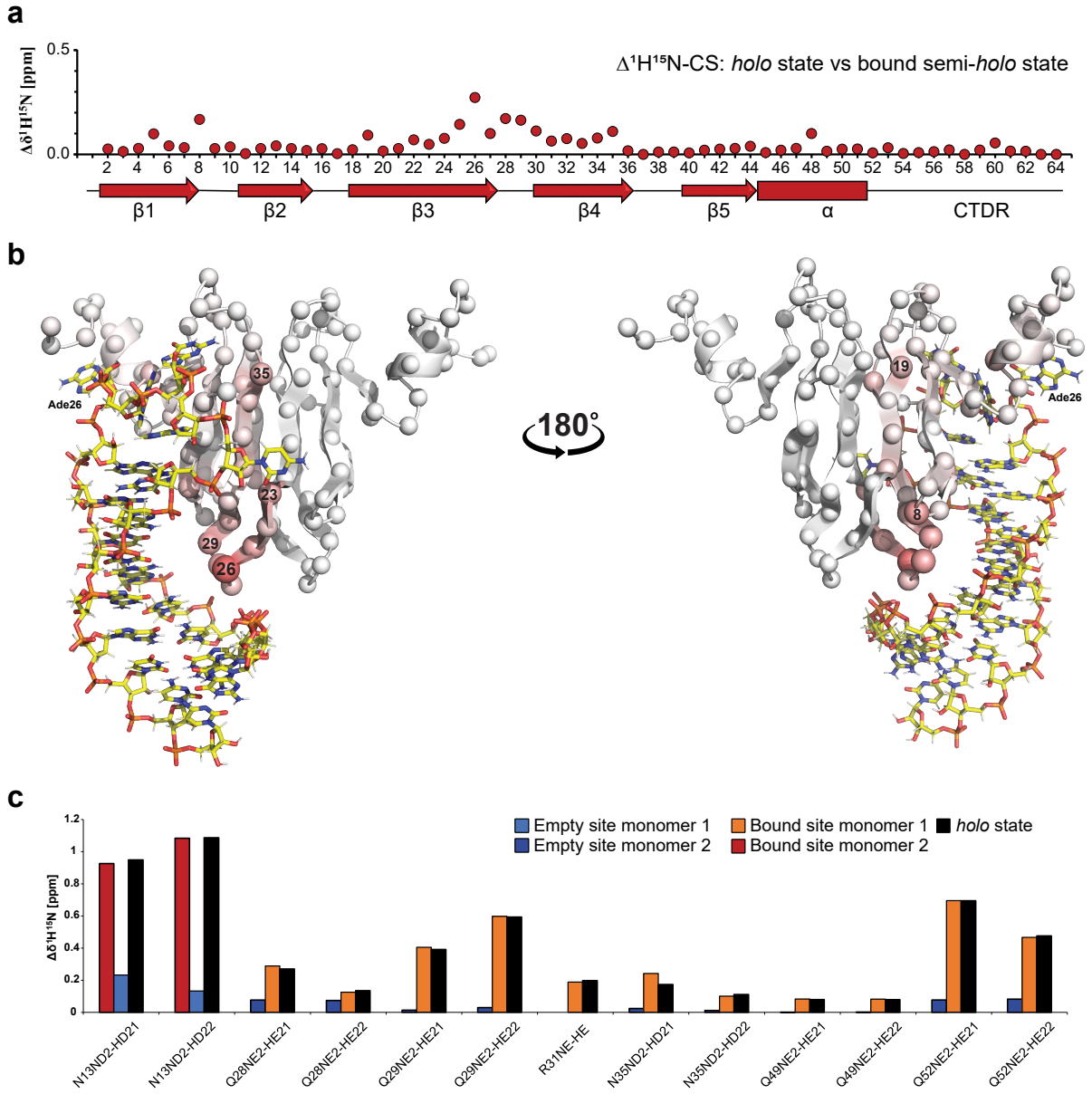

a, A dot plot with NH-CS differences between the bound site of the semi-*holo* SL2-RsmE dimer complex and the *holo* complex. The letter P indicates proline residues. **b,** The same NH-CS differences were projected onto the semi-*holo* SL2-RsmE dimer complex and they are shown for both the bound and empty sites. Intensity of red colour and diameters of spheres correlate with the magnitude of amide CS difference at every RsmE residue. **c**, Bar plot with the $^{1}H^{15}N$-CSP of side chain amides of the RsmE dimer upon binding to one (semi-*holo*) and two (*holo*) SL2 RNAs. Considering that the binding sites are composed of residues from both RsmE monomers, the bars from the semi-*holo* state are differently colour-coded for the two monomers (light and dark colours) and the two binding sites (blue/dark blue and red/orange colours).

Supplementary Fig.7: Chemical shift changes of the side chain amides of RsmE dimer upon binding to one 4bpSL2 RNA.

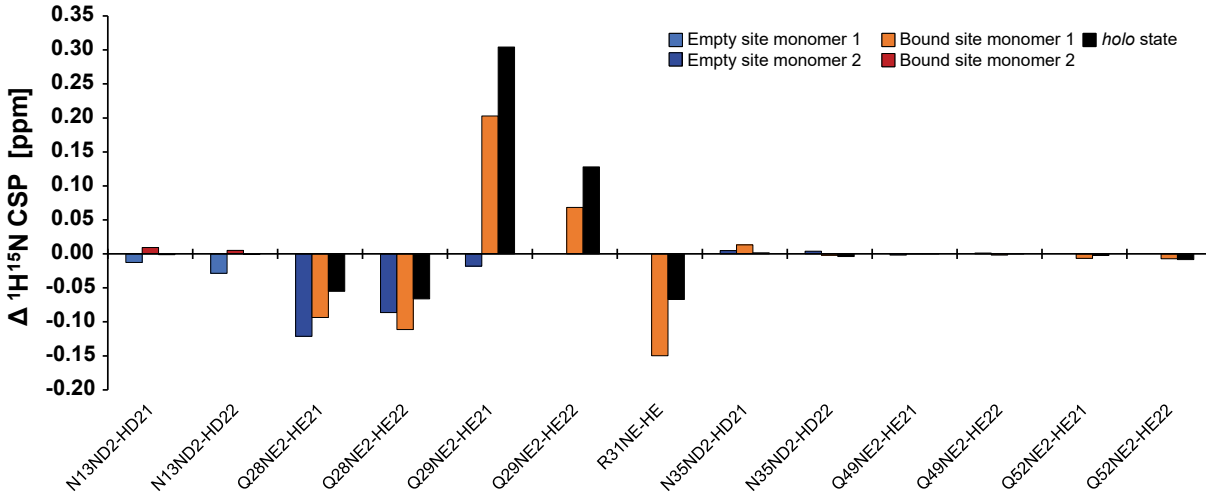

Bar plot showing the difference between the $^{1}H^{15}N$-CSP triggered by the binding of one 4bpSL2 RNA and one SL2 RNA on the side chain amides of the RsmE dimer. Computed as: $\Delta\ ^{1}H^{15}N$ CSP = SL2-RsmE dimer $^{1}H^{15}N$ CSP − 4bpSL2-RsmE dimer $^{1}H^{15}N$ CSP. The same quantification was performed for the two *holo* states (Black bars).

Supplementary Fig.8: Line-broadening of backbone amide peaks in residues from the empty binding site of the RsmE dimer.

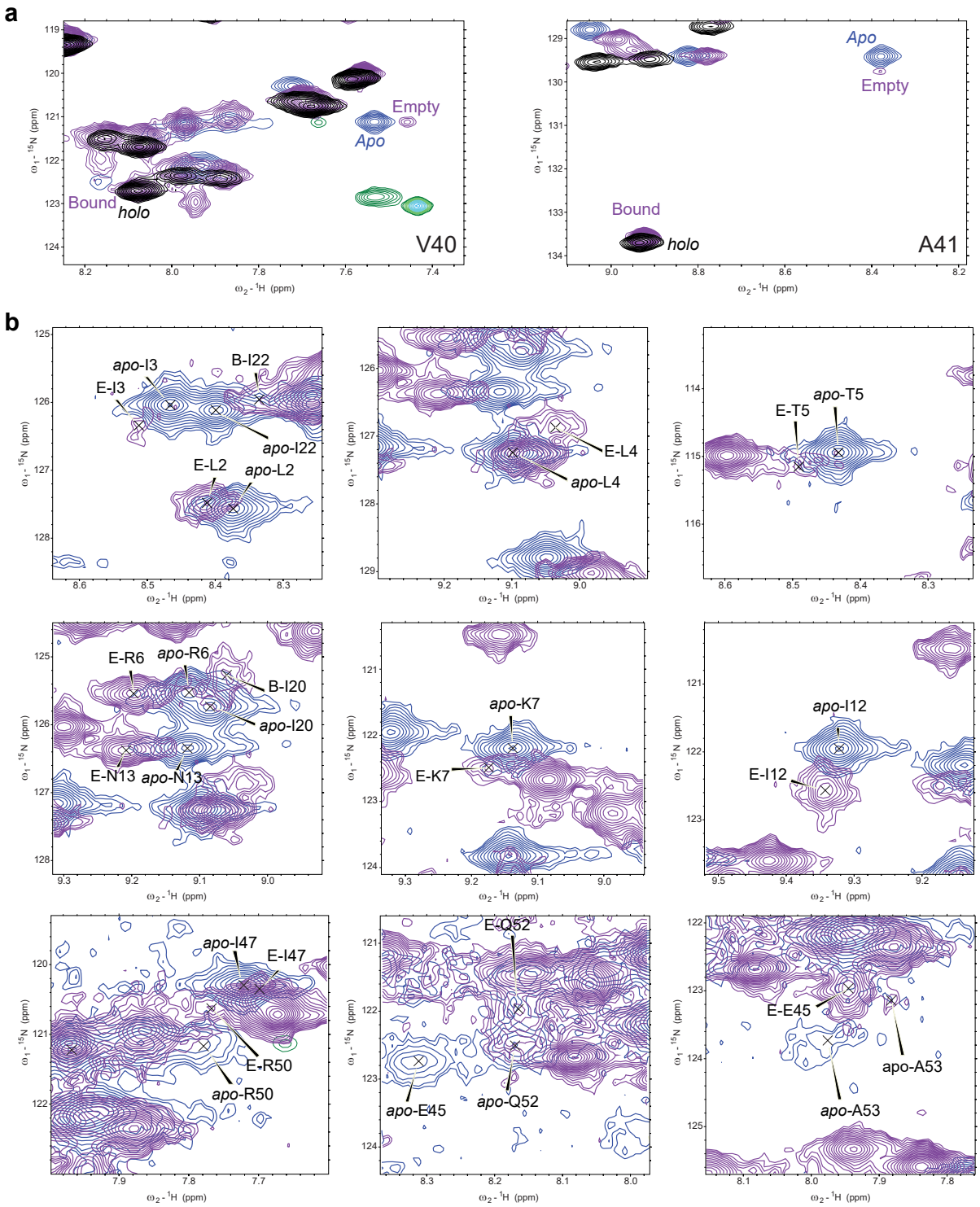

a, Overlay of V40 and A41 amide peaks in the $^{1}H^{15}N$-HSQC spectra of the RsmE dimer in its *apo* state (blue) and the semi-*holo* (purple) and *holo* (black) SL2-RsmE dimer. **b** Overlayed $^{1}H^{15}N$-HSQC spectral regions of the *apo* RsmE dimer (blue) and the semi-*holo* SL2-RsmE dimer complex (purple) for selected amide signals. Backbone amide peaks that experienced line-broadening are labelled.

Supplementary Fig.9: Upon binding to one SL2 RNA, some CS in the α-helix of the empty binding site of RsmE dimer move towards the random coil chemical shift.

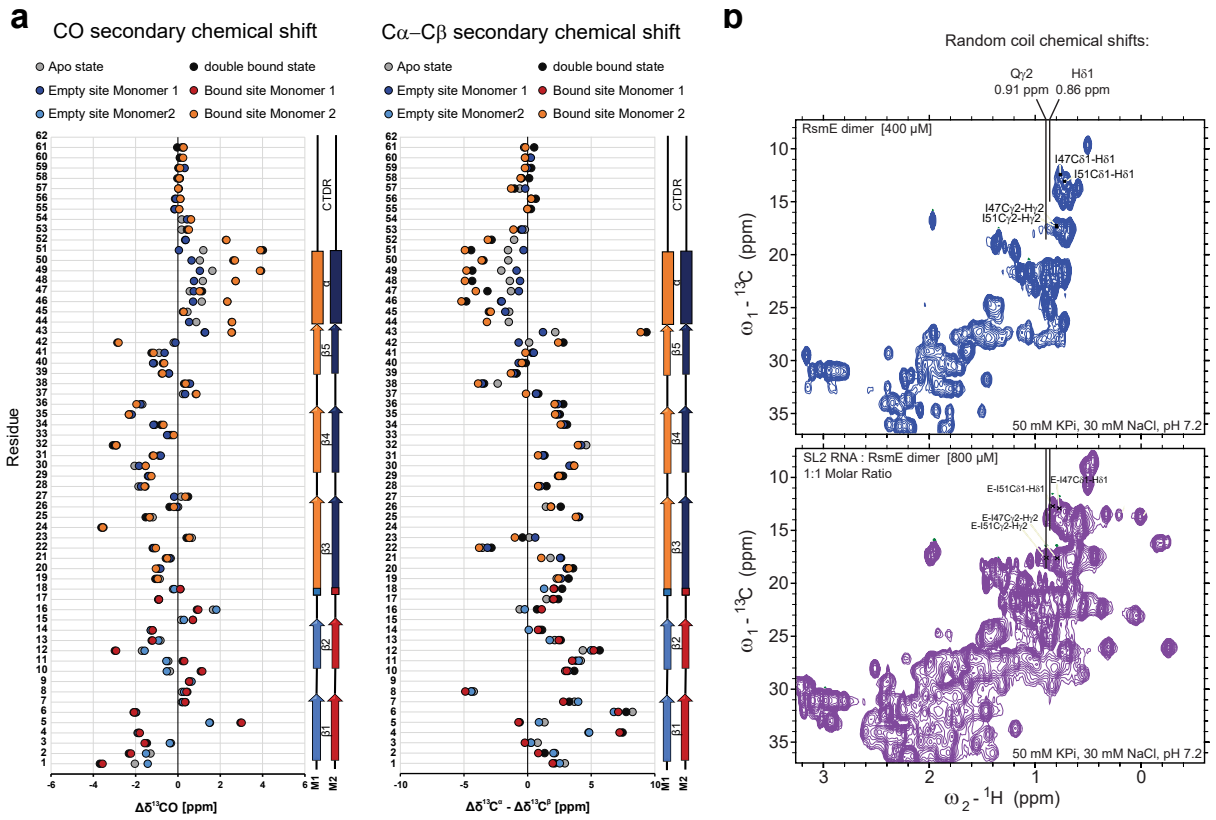

a, Two dot plots with the CO and Cα−Cβ chemical shift difference to the random coil CS in the *apo* RsmE dimer (grey), semi-*holo* SL2-RsmE complex (red, orange and blue) and *holo* complex (black). The differences from the semi-*holo* complex are colour-coded: warm colours (orange and red) correspond to residues on the bound site, cold colours (light blue and dark blue) refer to the empty site. The zero line (black) indicates the random coil chemical shifts. **b,** Methyl region of $^{1}H^{13}C$-HSQC spectra from the *apo* RsmE dimer (top, blue) and the semi-*holo* SL2-RsmE dimer (bottom, purple). Labels indicate I47 and I51 methyl (Hγ2 and Hδ1) peaks from the α-helix in the empty binding site of RsmE dimer. Random coil chemical shifts for Isoleucine methyl ^{1}H are indicated with black vertical lines.

Supplementary Fig.10: The α-helix of the empty binding site loses its contact with the β-sheets in the semi-*holo* SL2-RsmE dimer complex.

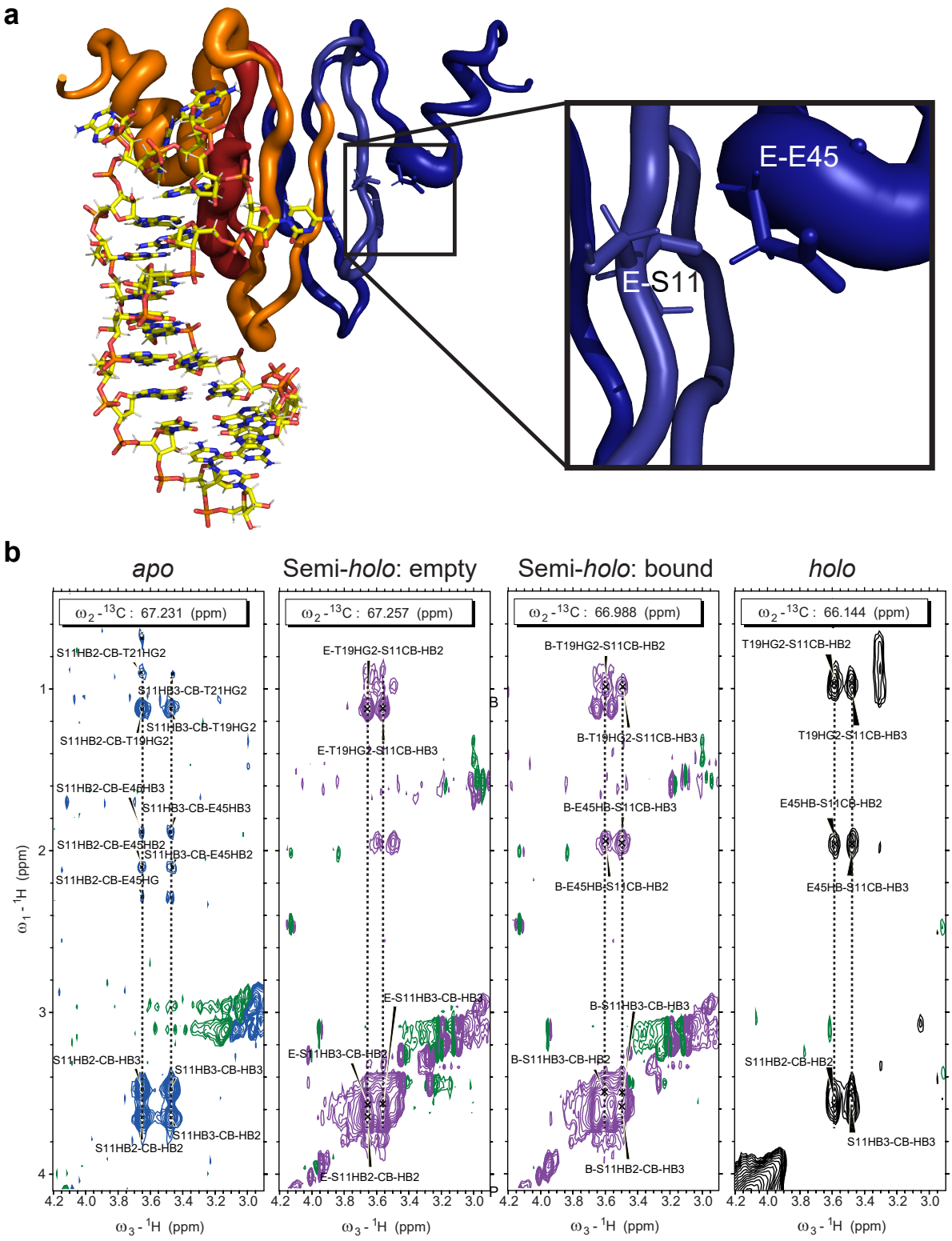

a, RsmE dimer depicted as a tube of variable width where tube thickness is proportional to NH CSPs. Contact between β-sheet and α-helix is mediated by residues S11 and E45. Coordinates for structure are derived from the SL2-RsmE dimer complex (PDB:2mfe). The sidechains of residues S11 and E45 in the empty site are shown. Insert shows an expanded view of these residues. **b**, Regions of the ^{13}C-resolved NOESY for the *apo*, semi-*holo*, and *holo* SL2-RsmE dimer complexes showing NOEs between S11 Cβ-Hβ2 and Hβ3 and E45Qβ protons.

Supplementary Fig.11: The *apo* RsmE dimer undergoes a temperature-dependent structural transition.

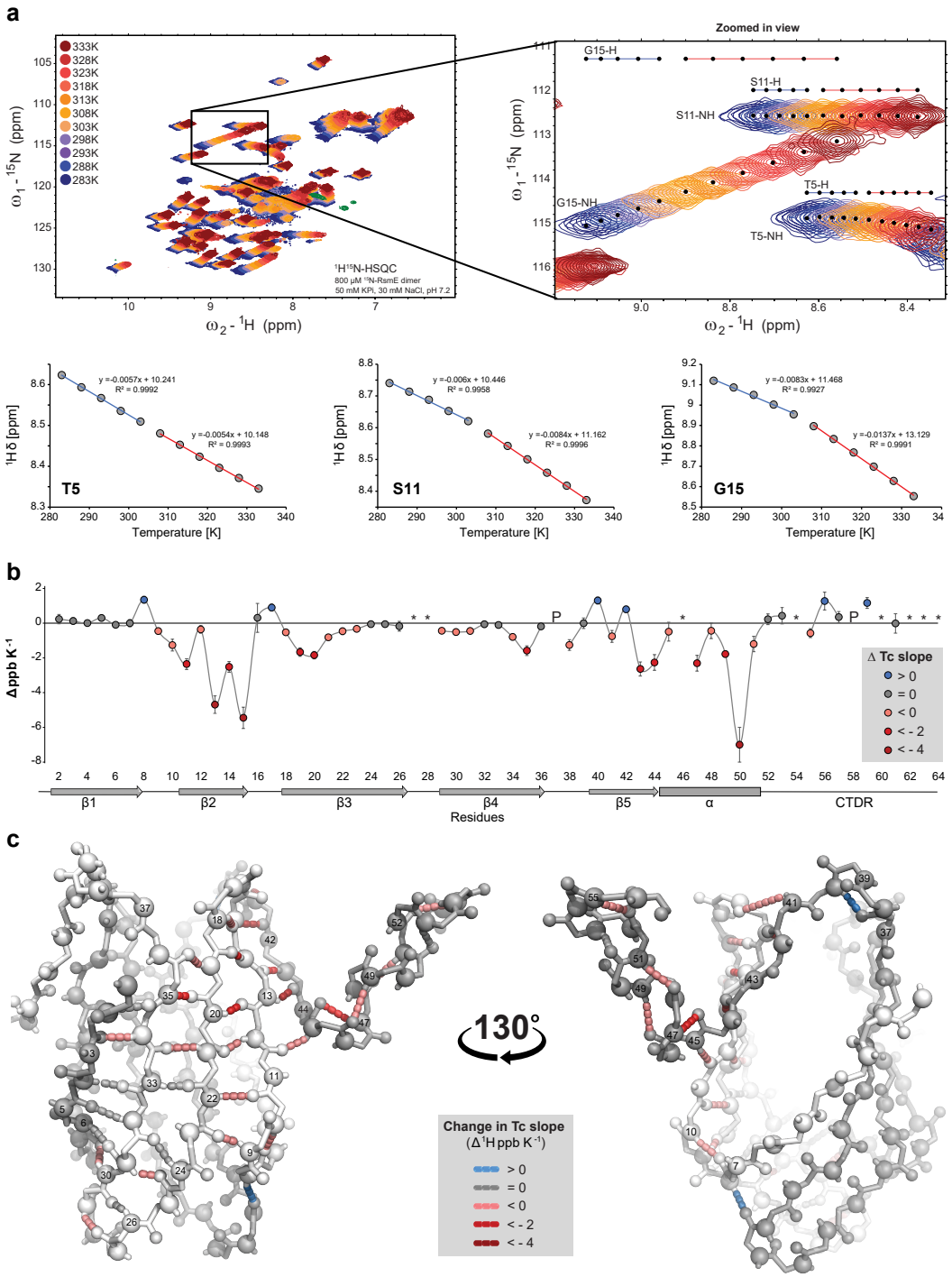

a, Overlaid $^{1}H^{15}N$-HSQC spectra of the RsmE dimer at different temperatures (283K to 333K). Three dot plots show amide proton CS temperature dependencies from three NH peaks. S11 and G15 showed non-linear temperature dependence with two linear regions at low and high temperature (temperature coefficients are given as Tc @<303K and Tc @ >308K). **b**, Dot and line plot indicating the changes in Tc (= Tc @<303K – Tc @>308K in Δppb K^{-1}) plotted versus residue position in the *apo* RsmE dimer. A negative value corresponds to a more negative temperature coefficient for the conformation after the transition (> 303K). Stars (*) indicate backbone amides that are not observed at temperatures higher than 313K and therefore no change in slope could be calculated. The letter P marks proline residues. **c**, Cartoons of the backbone of the *apo* RsmE dimer. Monomers are differently coloured in light and dark grey. Segmented coloured lines correspond to hydrogen bonds that experienced non-linear temperature coefficients. The magnitude of the change in Tc is indicated by the colour scale.

Supplementary Fig.12: The binding of one SL2 RNA to RsmE dimer alters the hydrogen bonds in the β-sheets of RsmE dimer.

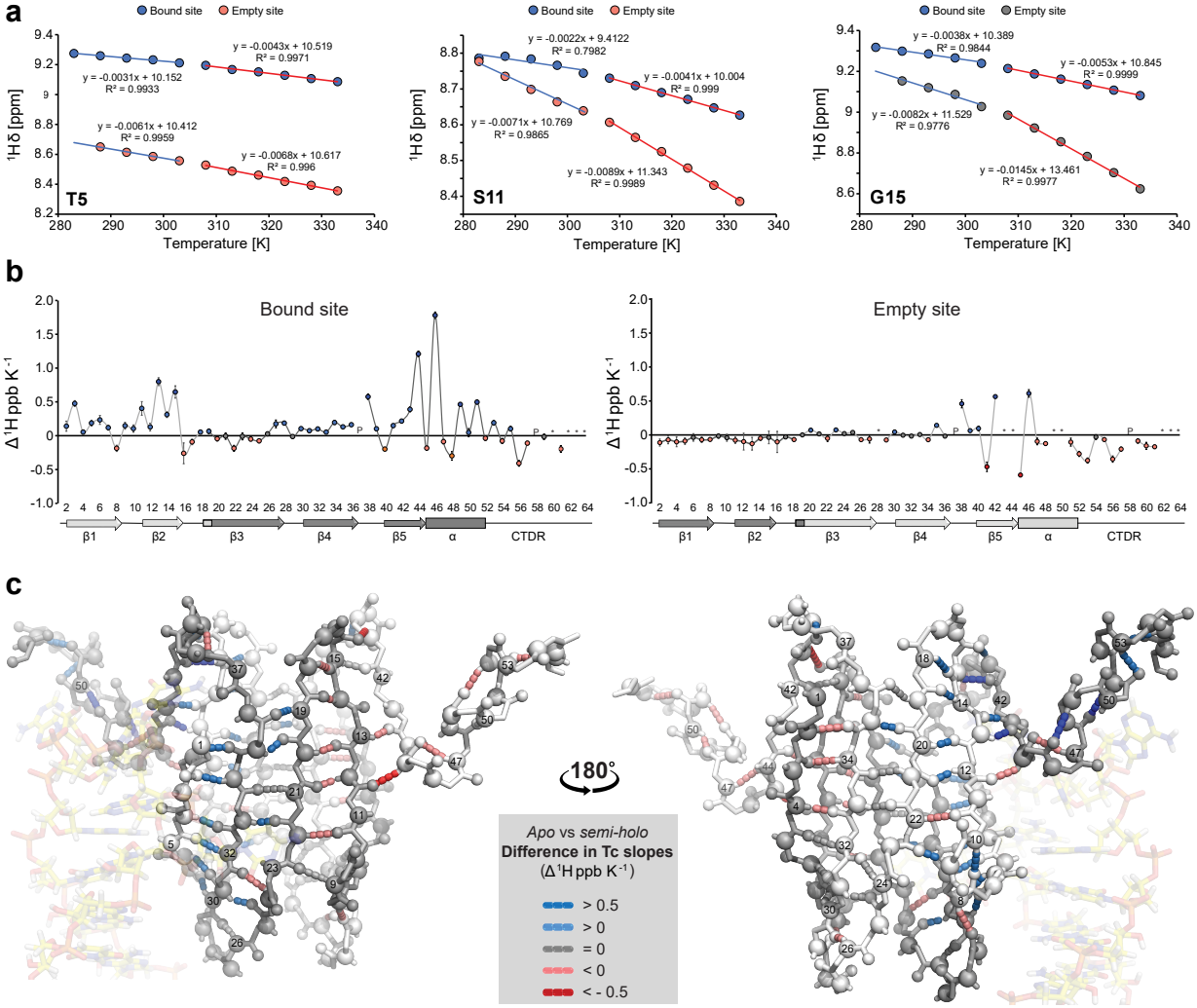

a, Three dot plots show amide proton CS temperature dependence of three H^N signals. They showed non-linear temperature dependence with two linear regions below 303K and above 308K. **b**, Two dot and line plots with the SL2 RNA-binding induced changes in temperature coefficient (ΔTc in ppb K^{-1}) plotted versus residue position for bound and empty sites of the RsmE dimer (semi-*holo* state). ΔTc = [Tc@<303$K_{semi\text{-}holo}$ + Tc@>308$K_{semi\text{-}holo}$] – [Tc@<303K_{apo} + Tc@>308K_{apo}]. A negative value corresponds to a more negative Tc for the semi-*holo* state. Stars (*) indicate backbone amides that are not observed at temperatures higher than 313K for which ΔTc could not be calculated. The letter P marks proline residues. **c**, Backbone atoms of the semi-*holo* SL2 RNA-RsmE dimer state. RNA is rendered transparent to ease RsmE dimer visualization. Monomers are differently coloured in light and dark grey. Interrupted coloured lines correspond to hydrogen bonds that experienced significant changes ($p<0.05$) in the Tc after binding of the first SL2 RNA. The magnitude of the change in Tc is indicated by the colour scale.

Supplementary Fig.13: The hydrogen-deuterium exchange curves of the backbone amides in the *apo* RsmE dimer and in the semi-*holo* SL2-RsmE dimer complex.

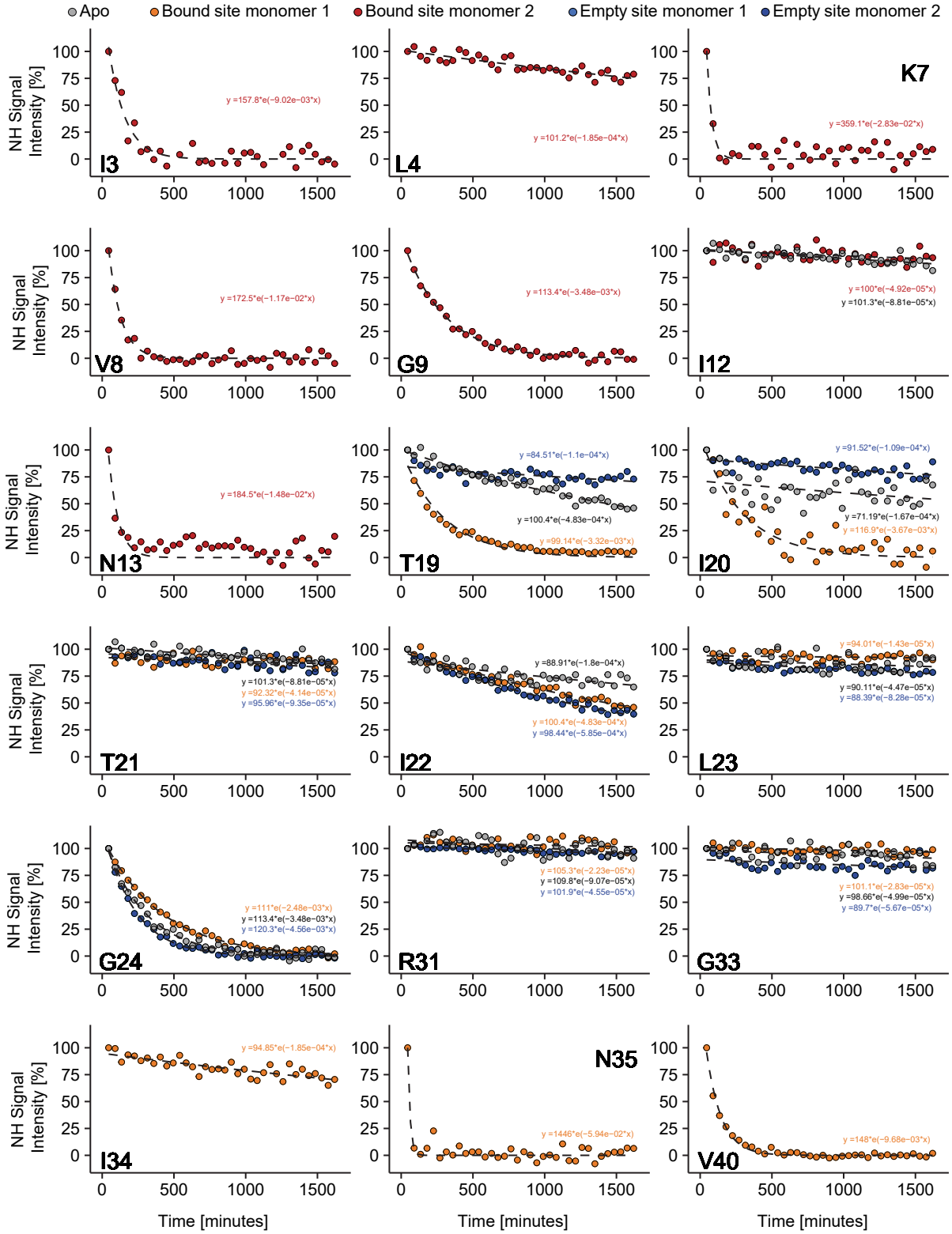

Observed HDX curves for well-resolved peaks of the backbone amides of the *apo* and semi-*holo* RsmE dimer states. Data are coloured-coded following the colours in the RsmE monomer schemes in Fig.1,3 and 4. HDX curves of R6, E10, I14 and I32 are shown in Fig.5c.